High-Performance Transparent Electrodes for Automobile Windshield Heaters Prepared by Combining Metal Grids and Oxide/Metal/Oxide Transparent Electrodes

Woo-Seok Cheong, Young-Hoi Kim, Joon-Min Lee, Chan-Hwa Hong, Ho-Yeol Choi, Young-Jin Kwak, Young Jun Kim, and Young Shin Kim*

Transparent heaters can be fabricated with a wide variety of materials including indium-tin oxide, carbon nano tubes, graphenes, metal nanowires, metal grids, and hybrid-type electrodes. However these materials have been applied to small area heaters below 0.01 m^2 because of the limit of electrical and optical properties. High-performance transparent electrodes for large-area purpose (over 1.0 m^2) have never been developed with any practical applicability in spite of their utility for removing fog or iced water on automobile windshield, which can be critical for safety and convenience of the drivers. Achieving ultralow resistance with high transparence is the major technical barrier in windshield heaters due to the intrinsic long distance between electrodes and low battery voltage in automobiles. In this study, a high performance transparent electrode, super hybrid electrode (SHE) is developed, which is manufactured by combining metal grids with oxide/metal/oxide electrode based on a newly developed electroplating method, which guarantees uniform properties over large area, over 1.0 m^2. Utilizing this newly devised electrode technology, an automobile windshield heater is successfully fabricated with sheet resistance of 0.1–0.3 Ω $\square^{-1}$ and the transmittance of over 82% in large area samples of 1.01 m^2, which is good enough for automobile windshield application.

1. Introduction

Transparent conductive electrodes (TCEs) have been developed as important electronic materials in industrial fields for flat panel displays including liquid crystal display (LCD), active matrix organic light emitting device (AMOLED), and thin film solar. Recent expansion of TCEs' applications in new area such as smart-board touch screen panel (TSP) and transparent heater for automobile windshield requires further improvement in their electrical and optical properties.[1,2]

Prof. W.-S. Cheong, Y.-H. Kim, J.-M. Lee, Dr. C.-H. Hong, H.-Y. Choi, Dr. Y.-J. Kwak, Dr. Y. J. Kim
Electronics and Telecommunications Research Institute (ETRI)
Daejeon 34129, Korea
E-mail: cws@etri.re.kr
Y. S. Kim
DaeKi Hi-tech Co
Daejeon 34367, Korea

DOI: 10.1002/admt.201800550

One of the most promising applications of TCEs is a large-area transparent heater on the front window in automobiles, which allows convenient removal of fog on the indoor side of the windshield and frost on its outdoor surface. Considering that windshield fogging frequently occurs during driving, convenient way of fog removal on windshield can be directly related with safety of the people on board. Moreover, recent trend in the increasing demand of electrical automobiles is expected to generate a huge market for TCE technology, since electrical automobiles do not come with the air-blowing system, which is used in defogging and defrosting on windshield. Generally, it is understood that the critical technology in transparent heater is to achieve ultralow sheet resistance below 0.5 Ω $\square^{-1}$, while keeping the transmittance over 70% at the same time. Since the voltage of automobile batteries ranges only 12 to 16 V, the area of the most automobile windshields is over 1.0 m^2 and the gap between electrodes is over 700 mm,[3] achieving low-enough sheet resistance to be viable for real application is understood to be a difficult mission. As far as we have done searches in the related fields, no TCEs have been developed that can satisfy all those specifications at the same time.[2]

Up until now, indium-tin oxide (ITO) has been most widely used in TCE industry. However, even with high optical transmittance reaching 90%, ITO has not been successful in application for automobile windshield due to relatively high sheet resistance (10 to 100 Ω $\square^{-1}$).[4–6] Recent need for TCE technology introduced three different candidate materials including carbon-based materials, metal nanowires (NWs), and metal grids. Although carbon-based materials including carbon nanotubes (CNTs)[7–11] and graphene[12–14] has some advantage in flexibility, CNTs and graphenes have relatively high sheet resistance and low optical clarity compared with ITO. Among metal NWs,[15–21] silver nanowires (Ag NWs) have been improved greatly in recent years with their sheet resistance reaching around 30 Ω $\square^{-1}$, while keeping the transmittance up to 90%. However, a severe optical problem like "haze"

is unavoidable, as thickness of Ag NW coating is increased to achieve low sheet resistance.

In the case of metal grids, the artificial structures for decreasing sheet resistance using low resistivity metals (Cu or Ag) can be manufactured with almost no limit of resistance via control over mesh dimensions. From a practical viewpoint, however, not only does the low resistance fabrication process, that is deposition of thick metal film (by sputter) and wet-chemical etching of the patterned metal films, hard to guarantee uniform micrometer-scale metal grid, but also cause high cost and severe environmental hazards. Recently, in an effort to avoid those disadvantageous processes, a variety of new methods, electrohydrodynamic (EHD) jet printing,[22] metal imprint,[23] solution grown (electroless plating) mesh,[24] and electroplated mesh[25] were introduced. However these technologies also are involved with some characteristic demerits including impractically small in sample area, high sheet resistance, and incompatibility of the process for mass production. Electrospun metal nanofibers[26–28] have attracted much interest enabling production of flexible TCE films with random network pattern and the low resistance. In different methods, the random metallic networks were fabricated based on the following two processes; one was related with cracking a sacrificial layer, metal deposition and lift-off of the sacrificial layer,[29–31] and the other was about self-assembled Ag networks.[32,33] However, still these metallic networks could not perform low-enough sheet resistance as to be applicable for practical purpose.

In order to improve optoelectrical properties and flexibility, many different types of hybrid TCEs including Ag grids on ITO,[34] Ag grids on graphene,[35] graphene/Ag NWs/graphene,[36] Ag NWs on conductive polymer,[37] metal mesh on graphene oxide,[38] NWs on graphene,[39] electrospun nanofiber on graphene[40] had been developed. Furthermore, An et al. reported hybrid TCE films with excellent sheet resistance and optical transmittance using electrospinning and electroplating methods.[41] Jang et al. developed a new hybrid-type flexible TCE substrate by merging surface-embedded Ag NW with electroplated Ag grids.[42] It is worthy to take note of the electroplating technology, which had been utilized in both of the hybrid TCEs for achieving low sheet resistance.

In the related studies, transparent heaters had been fabricated using both singular TCEs,[2,5–14,16,20,30,43] or hybrid TCEs.[35,37] Most of these heaters were either small in size with their area below 0.01 m^2, or only heating performance were reported without mentioning size of the devices, which is a key information when it comes to real applicability, in which large active device is required as in windshield application for automobile. Application for front windows in automobiles requires transparent heaters with ultralow resistance, manufacturability in large area over 1.0 m^2, and low battery voltage. These multiple technical standards can hardly be achieved with the TCE technologies described above.

In an effort to find practical application for automobile windshield, tungsten wires had been used instead of TCEs, where wires with diameter of about 28 μm were inserted between laminated glasses of the front window. However, this method induced "spring haze" over windshield, preventing approval in most of the countries due to major safety issue. Saint-Gobain Glass Co. (France) produced multilayered TCEs, OXMYOXMYOXMYOXMYO (M = Ag, O = oxide, X and Y = diffusion barrier materials) with sheet resistance of about 1.0 Ω $\square^{-1}$ and transmittance of about 70%.[43] This multilayered structure basically came from "OMO(oxide/metal/oxide)" structure, which is a transparent electrode with good sheet resistance and optical properties, typically of 5–10 Ω $\square^{-1}$ and 85–90%, respectively.[44,45] However, since the sheet resistance is not low enough to be run by the normal automobile battery, Saint-Gobain Glass Co. uses a transformer to amplify the voltage at least two to four times for effective operation.

In this study, we presented a newly developed electroplating method, which enabled manufacturing the hybrid electrode, "SHE (super hybrid electrode)," with superb TCE performance in addition to scalability to a large-enough device as to be applicable to commercial automobiles. Major structural feature of SHE is the combination of metal grids with OMO transparent electrode. The key aspect of the novel electroplating technology is that it enables the uniform growth of the partially embedded metal grids on OMO which enabled ultralow sheet resistance.

2. Results and Discussion

In an effort to manufacture a commercially viable windshield that can conveniently remove fog and frost in automobile windows without resorting to the conventional air-blowing method, we developed a new electroplating technology that enables manufacturing large-area TCE with ultralow resistance that can run on a small battery voltage.

Figure 1a represented a schematic description on manufacturing concept of the super hybrid electrode (SHE) developed in this study. SHE was produced by simple combination of OMO electrode with metal grids. The key point is that the metal grids were formed by a unique electroplating method, in which the sandwiched metal layer between oxide layers works as a seed film for growing metal grids. Figure 1b is a conceptual description for the manufacturing process used to realize SHE in Figure 1a. First three layers of OMO is formed on glass or polymer film by sputtering method (Figure 1b(i)), on top of which photo-resist (PR) is coated (Figure 1b(ii)). After patterning PR (Figure 1b(iii)), metal part in OMO is exposed by etching away the top oxide layer (Figure 1b(iv)). Now metal is grown using electroplating method followed by removing PR (Figure 1b(v),(vi)). Although we used Ag for the metal layer in OMO, gold or silver alloy can also be used for this process.[45] As for the metal gird, among the many different types of metal candidates, Cu was used in this study.

Figure 2a is a microscopic image of the fine-pattern photomask with the line width of 2 μm and the line pitch of 100 μm, which was used to prepare SHE grid. Figure 2b shows the scanning electron microscope (SEM) image of the SHE structure produced by the procedure described in Figure 1b. The inset image is the enlarged view of the SHE grid at crossed area, which clearly shows successful growth of Cu grid using the electroplating method introduced in this study. Figure 2c,d are SEM images of the growing steps of the copper grids on the Ag seed layer of OMO which corresponds to the schematic step of Figure 1b(v). In this study ZTO/Ag/ZTO electrode was

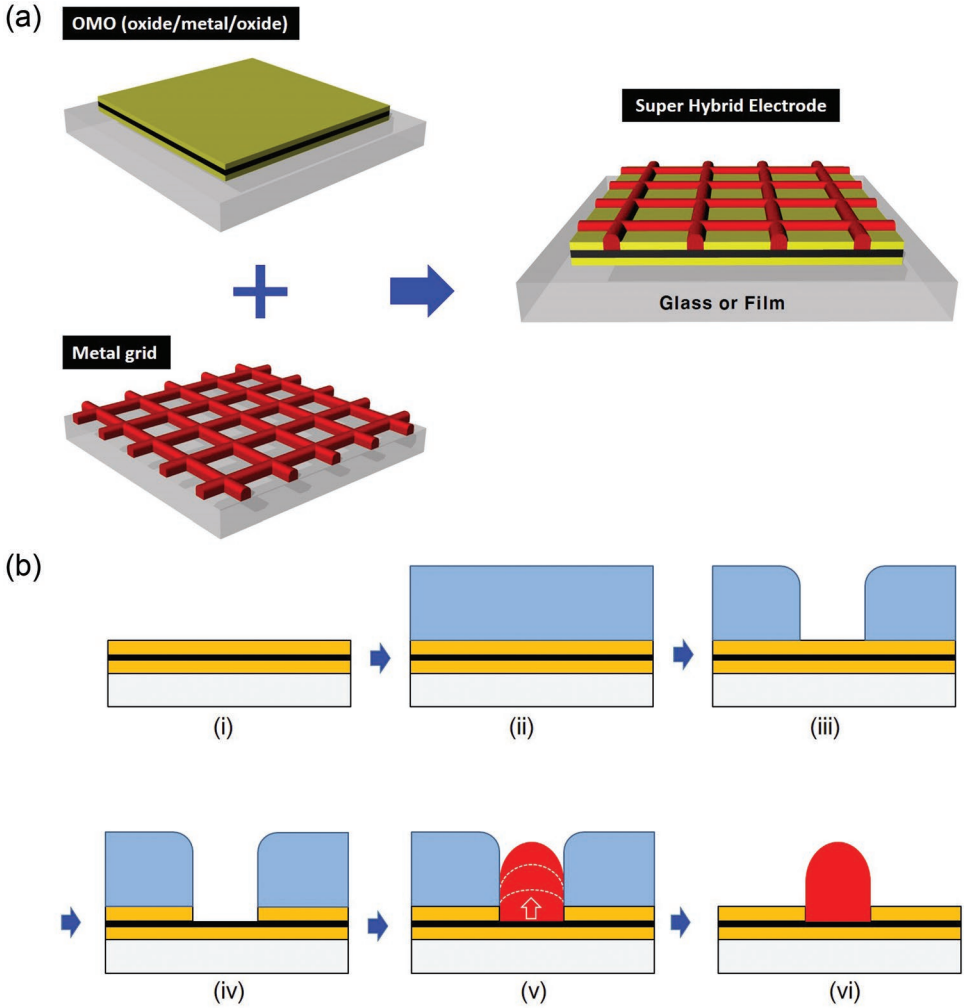

Figure 1. a) Schematic description on the design concept of SHE and b) procedures for manufacturing SHE; (i) deposition of oxide/metal/oxide layers on a substrate (glass, or film), (ii) coating photoresist, (iii) photolithographic patterning, (iv) selective-etching of the top oxide layer, (v) metal growing by the unique electroplating method, and (vi) stripping the photoresist.

used for the OMO layer. Figure 2c and 2d display the cross-section views of the copper grid grown for 60 s (≈0.5 µm of height) and for 200 s (≈2.0 µm of height seconds), respectively. In the electroplating deposition, the copper can be grown selectively on the exposed Ag seed line, since Ag is the only conducting surface. For the electroplating process, 1.0 wt% of Cu_2SO4 was used in deionized (DI) water at room temperature. Since the electroplating process follows Faraday's second law, where the depositing rate depends on current and mole fraction of the solution, generally the electroplating rate can simply be increased by increasing the concentration of the solution. Figure 2e is a side-view image of the SHE structure where the Cu grids (2.5–3.5 µm high) were grown for 300 s. On top of the Cu grids, the overgrown crystal structure can be observed. Figure 2f shows both the cross section and side view of the SHE grid, representing very smooth surface of its side.

Transmission electron microscope (TEM) images of the cross-section views of SHE are shown in **Figure 3**a–f. Figure 3a is a representative image of SHE cross section fabricated in this study, where the line width of Cu mesh was 1.97–2.24 µm and the height was ≈1.79 µm. Figure 3b is the enlarged view at the bottom center of the SHE in Figure 3a, which clearly shows Cu grown selectively on Ag/ZTO layer. It is worthy of taking note of the uniform thickness of each layer, with the thickness of Ag and ZTO being 12.96 and 29.40 nm, respectively. Figure 3c,d are bottom left and right corners of SHE in Figure 3a. At these bottom side areas, growth of Cu is observed to have occurred beneath the PR layer, which is thought to have occurred due to under-cut of 0.2–0.3 µm beneath PR during wet-etching process. Figure 3e is the enlarged view of top center area of the SHE cross section in Figure 3a. The preferred {111} crystal planes with polycrystalline structure can be clearly observed. Finally, Figure 3f shows the electron diffraction pattern of Cu SHE, which well supports the pyramidal shape ({111} plane) of the Cu crystal structure in Figure 3e.

In order to evaluate the crystalline structure of the copper mesh, three different samples (i), (ii), and (iii) prepared with varying the Cu growth time (100, 200, and 300 s) were characterized by X-ray diffraction (XRD) (Figure 3g). The common preferred orientation of Cu(111) plane appeared dominantly

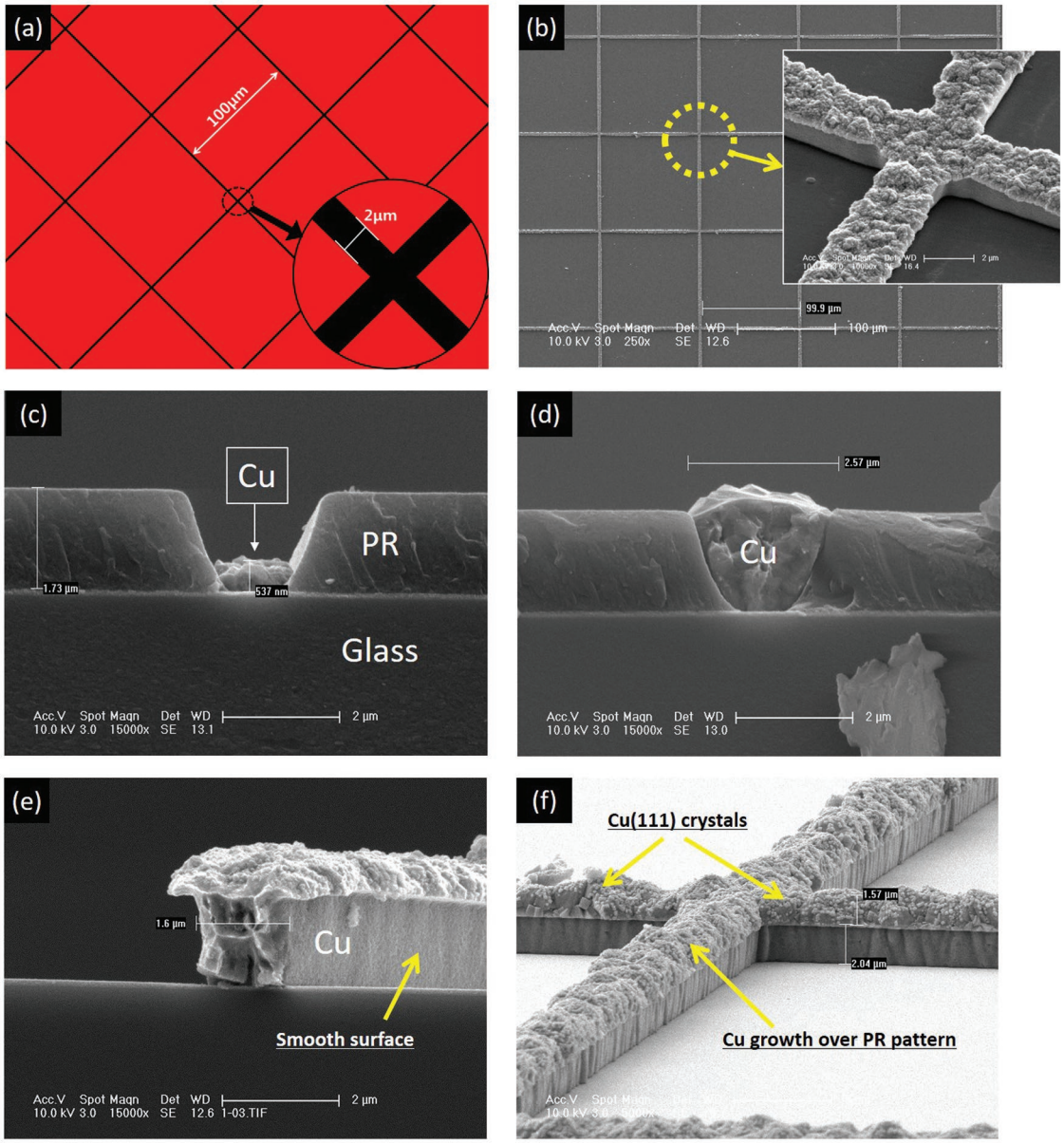

Figure 2. SEM images from the SHE process; a) photomask pattern with the line width of 2 μm and the line pitch of 100 μm, b) SHE Cu grids obtained busing the photomask, growth step of copper grids on Ag seed layer of ZTO/Ag/ZTO electrode at c) 60 s and d) 200 s, and e) side view and f) cross section of SHE structures at 300 s.

in all the samples together with minor peaks of Cu(220) and Cu(200) planes. The inset shows the enlarged shape view of the Cu(111) peak in the samples, where the 2-theta (θ) values ranged from 43.0° to 44.0°. The copper grain size was calculated based on the Scherrer's formula,[46] $D = 0.9\lambda/B\cos\theta$ where λ, θ, and B are the X-ray wavelength, Bragg diffraction angle, and full width at half maximum (FWHM). Since λ and θ are 0.154054 nm (Cu-Kα) and 21.69, respectively, B can be calculated to be 0.22° to 0.23°, which in turn would result in the average size of copper grains to be ranging from 45 to 47 nm.

In order to understand the efficiency of the electroplating method developed in our study, SHE grid was fabricated using a conventional electroplating method (glass size = 100 mm × 100 mm and thickness = 0.7 mm). **Figure 4**a(i) shows a schematic illustration of the conventional electroplating method, where a copper source plate was connected to an anode and a patterned OMO glass was connected to a cathode. Figure 4a(ii) is the image of an optical microscopy for the Cu grid manufactured by the conventional electroplating method, where many defects of broken Cu girds were indicated with white arrows. Figure 4a(iii) is an enlarged view of the cross line in Figure 4a(ii). Cu grew only partially leaving much of the edge area of Ag uncovered with Cu, suggesting limited nucleation and/or growth of Cu grains on Ag seed lines, suggesting limited electron density and low transfer rate. If the conventional electroplating method is applied to a large area

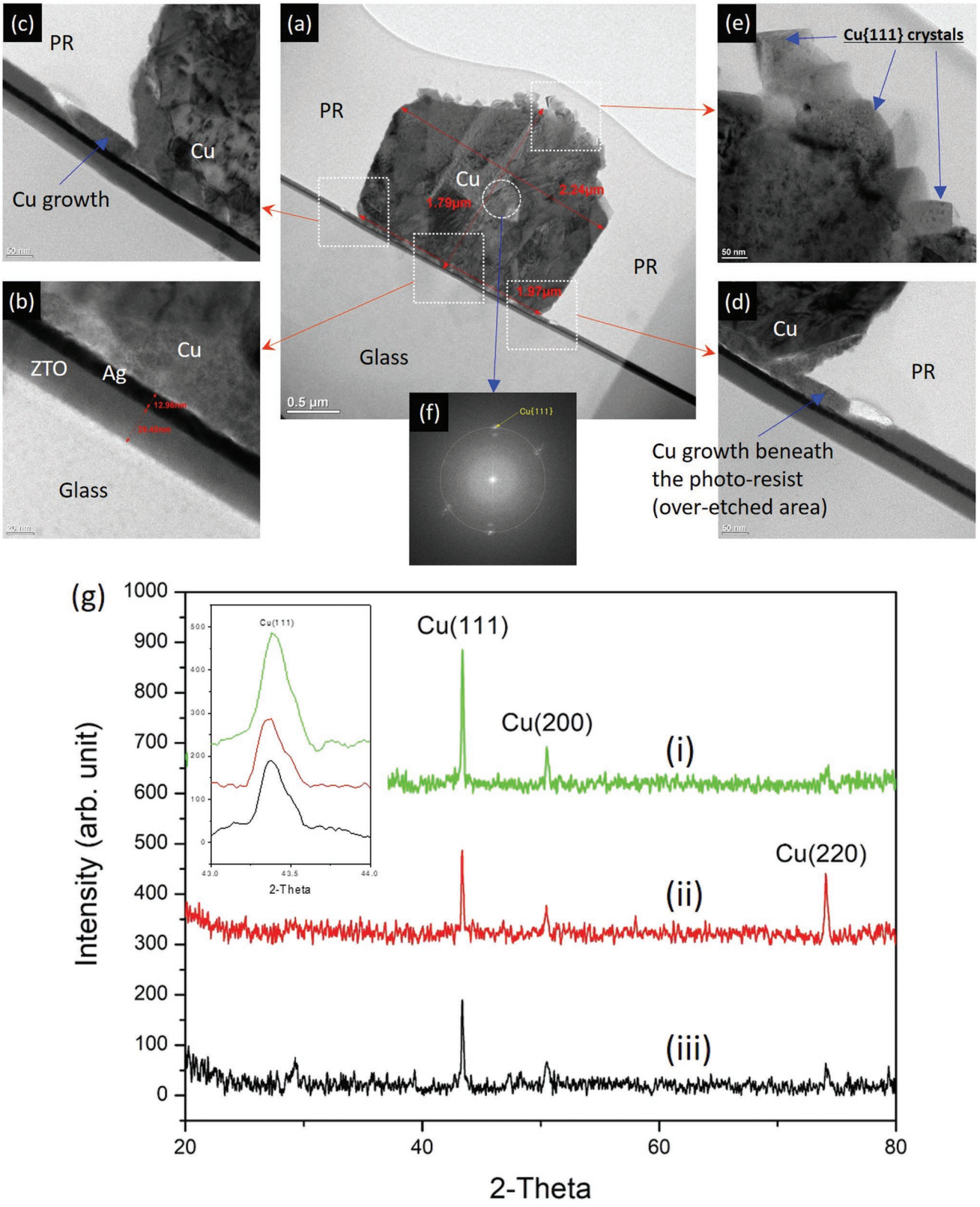

Figure 3. TEM images obtained from SHE; a) cross-section, enlarged views of b) the bottom center, c) bottom left, d) bottom right and e) top center position from the image (a). f) Electron diffraction pattern at center position of (a) and g) XRD results from the SHE samples with growth time of (i) 100 s, (ii) 200 s, and (iii) 300 s.

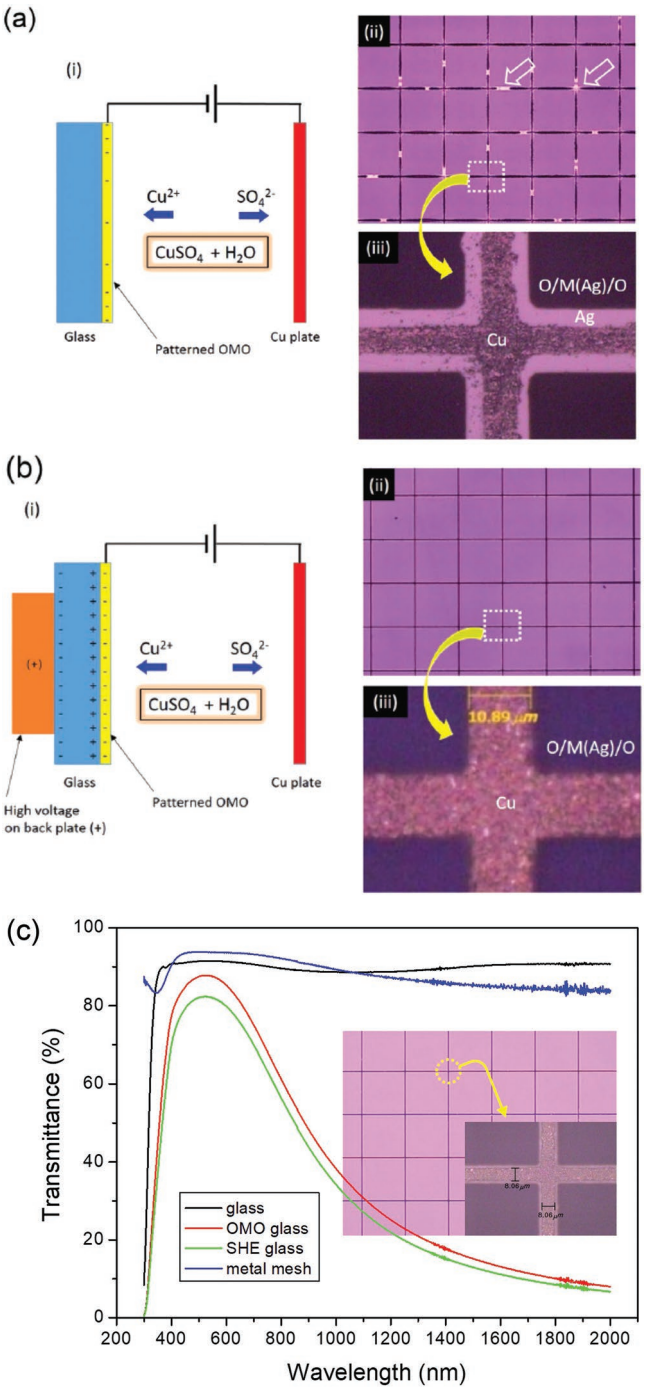

Figure 4. a) Conventional electroplating process; (i) schematic description of the Cu growth in the, (ii) an optical microscopy of the SHE sample obtained by the conventional electroplating method, and (iii) enlarged view at the cross-line area in (a-ii). b) Novel electroplating method for preparing SHE; (i) conceptual description of the newly developed electroplating method, (ii) an optical microscopy of the SHE sample obtained by the novel electroplating method, and (iii) enlarged view at the cross-line area in (b-ii). c) UV–vis spectra of the glass, OMO glass, SHE glass, and metal mesh (pitch = 100 μm, and width = 8 μm).

sample for practical purpose as in windshield of an automobile, low conductivity in the initial state would be more pronounced causing more imperfect Cu growth.

In order to overcome those limitations caused by the conventional method, a new electroplating method was devised. Figure 4b(i) shows the schematic illustration of the electroplating method developed in this study, where the only difference from the conventional method is use of ultrahigh positive voltage on the back plate of the patterned OMO glass. The positive potential on the back plate can align dipoles in the glass, producing plus charge on the interfacial surface of the glass, which is in contact with the patterned OMO. Polarization of the glass surface in turn attracts negative charges on the patterned OMO. Build-up of negative charges on the patterned OMO helps facilitate initial nucleation and growth of Cu grid by Cu^{2+} ions. As a result, nice and clean Cu mesh lines were formed without any hint of breakage as shown in Figure 4b(ii). Figure 4b(iii) shows enlarged image of the mesh-line cross, where the whole area of the Ag was covered by Cu with its line width measured to be 10.89 μm. The same process conditions, the electroplating voltage of 1.0 V, Cu_2SO_4 of 1.0 wt%, and growth time of 300 s, were used except the ultrahigh (+) potential of 15 kV on the back plate of OMO-patterned glass. More specific electrical mechanism of the electroplating with high voltage at the back plate requires further study in the future.

In order to see if this technique can be utilized to real applications, a large-area transparent heater was manufactured using this new electroplating method. Now a large-area heater was fabricated on a 24" glass, where the length and width of the heater was 520 and 310 mm, respectively, with its thickness of 1.1 mm. Figure 4c shows the UV–vis spectrum of the large-area SHE sample, where the pitch is 100 μm, and the width of copper mesh is 8 μm. The transmittance of the glass substrate (black line) was around 92% in the range of visible wavelength. The red line corresponded the transmittance of ZTO/Ag/ZTO glass, which showed excellent transmittance in the visible range (maximum transmittance of 87.8% at 530 nm) with steep and moderate decrease in UV and IR region, respectively. These optical properties are especially beneficial for automobile windshield application since the low transmittance in both UV and IR region would provide added merits of protecting drivers from UV light as well as blocking IR heat transfer through the windshield.[1] The maximum transmittance of the SHE glass (green line in Figure 4c) was 82.4% at around 530 nm. The metal mesh was positioned between OMO and SHE glass as indicated in blue line in Figure 4c. The transmittance of the metal mesh reduced gradually in the IR range with concomitance of scattering. Transmittance in visible light ranged from 90.4% to 93.9%. Theoretical value of the mesh transmittance (or the open area ratio) can be calculated from the pitch, and the width of the copper mesh, while the sheet resistance can be extracted from the transmittance (%), the height (μm) of the mesh, and the resistivity of copper (1.724×10^{-6} Ωcm). Transmittance of the copper mesh with a pitch of 300 μm and a width of 8 μm is calculated to be 94.7%, which is in close agreement with that of our result. Also sheet resistance is expected to 0.13 Ω $\square^{-1}$, when height of the mesh

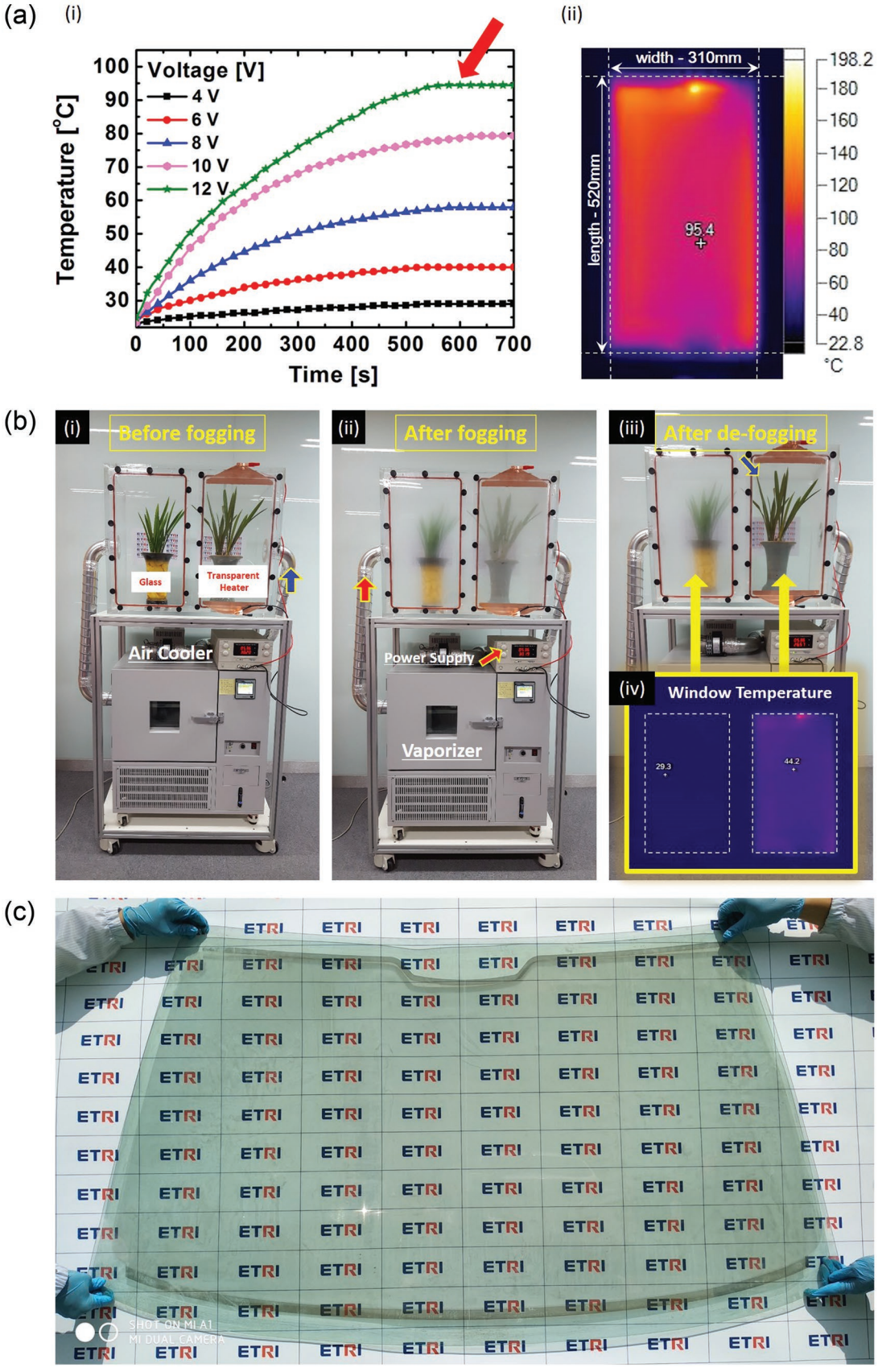

line is 2.5 μm as shown in the calculated values of the sheet resistance (S1, Supporting Information), which suggests controllability of the sheet resistance simply by changing those variables.

Figure 5a shows the heating test results of the large-area transparent heater (520 mm × 310 mm). When voltage was applied from 4 to 12 V, change of the temperature was monitored by an IR temperature detector (Figure 5a(i)). For all the voltage values used in this experiment, the temperature rose gradually with the rate of temperate rise higher for higher voltage. At 12 V, the saturated temperature was 95.4 °C as shown in Figure 5a(i) (as indicated by the red arrow). Also the image of the IR temperature of the large-area heater in Figure 5a(ii) shows uniform temperature profile all over the heater surface. In **Table 1**, major parameters (P_T, P_D, R_L, and R_S) were extracted from the results of the temperature dependence on voltage (Figure 5a(i)) base on Equation (1).[3]

Table 1. Major parameters (P_T, P_D, R_L, and R_S) extracted from the results of the temperature dependence on voltage (Figure 5a(i)) base on the Equation (1).

Voltage [V]	Current [A]	Sat. temp. [°C]	P_T [W]	P_D [W]	R_L [Ω]	R_S [Ω □$^{-1}$]
4	9.5	29	38	0.024	0.4211	0.2429
6	13.9	40	83.4	0.053	0.4317	0.2491
8	17.7	57.9	141.6	0.091	0.452	0.2608
10	21.1	79.3	211	0.135	0.4739	0.2734
12	24.5	94.5	294	0.188	0.4898	0.2826

$$P_D = V^2/\left(R_S L^2\right),\ R_L = R_S L/W,\ \text{and}\ WL = P_T/P_D \quad (1)$$

where P_D = power density; V = applied voltage; L = length between electrodes; W = width of the heater; P_T = total power of the system; R_L = resistance between electrodes; R_S = sheet resistance of the heater.

It is evident, based on the equation, that R_S should decease when V is low and L is large, which is the case with the most commercial automobiles, where battery output voltage (V) ranges from 12 to 16 V and height of windshield (L) is from 50 to 100 cm. Based on the results in Table 1 and S1 in the Supporting Information where R_S was 0.24–0.28 and 0.13 Ω □$^{-1}$, respectively, the real resistivity of the copper grids (≈2.5 μm high) fabricated by the electroplating method was about two times larger than that of the theoretically calculated value.

In order to evaluate the efficiency of the large-area transparent heater (L = 520 mm, W = 310 mm), a test bed was manufactured, which was equipped with an air cooler and a vaporizer to generate fog (Figure 5b). A transparent polyacryl chamber with two openings, one for a normal glass and the other for the transparent heater glass, was prepared. Inside of the chamber, two pots of orchid were positioned each right behind the two glasses. First, cool air was transferred into the test chamber from the right side to lower the temperature of the two glasses (Figure 5b(i)). Second, humid air was transferred into the chamber from the left side, instantly generating fog on both glasses (Figure 5b(ii)). Finally, 12 V was applied on the transparent heater, causing defog in 50 s (Figure 5b(iii)). When defog occurred on the SHE, the temperature of SHE was 44.2 °C while that of the normal glass was 29.3 °C. It turned out that increase in temperature up to 44.2 °C was sufficient enough to remove all water drops on SHE. Additionally, the temperature profile on SHE surface was very uniform as confirmed by the IR image in Figure 5b(iv).

Finally, a windshield equipped with SHE applicable to a real automobile was successfully fabricated. The manufacturing processes including photolithography, coating, etching, and electroplating steps, optimized for this study proved to be applicable for large-size product. Figure 5c shows the front window of a real automobile (Hyundai-Sonata) incorporated with SHE heater, where the length between the electrodes is 751 mm, the diagonal length is 1530 mm, and the total heating area is 1.01 m^2.

3. Conclusions

Low sheet resistance is an essential feature in applying transparent electrodes for automobile windshields, since low battery voltage and large gap between electrodes are the intrinsic parts of the automobiles of today. For this purpose, the SHE, which is in the form of metal mesh embedded in OMO structure, was successfully fabricated in large-enough scale utilizing a newly developed electroplating method. In this new electroplating process, ultrahigh voltage was applied on the back side of SHE substrate, which in turn generated concentrated negative charges on OMO, which as a result enabled uniform growth in metal grids.

The scalability of this process was confirmed by enlarging SHE structure from 5.6" (100 mm × 100 mm) to 24", and finally to over 60", which is the dimension of a commercial automobile windshield (Sonata, Hyundai). Using a custom-designed test bed, the ZTO/Ag/ZTO transparent heater with its sheet resistance of 0.24 Ω □$^{-1}$ and electrode gap of 520 mm, proved to efficiently remove small water droplets in the test-bed experiment within 50 s. High transmittance of 82.4% in the viable range but low transmittance in the UV and IR range is

Figure 5. a) Results from heating tests of the SHE heater (520 mm - L/310 mm - W); (i) plots of the resulting temperature against the heating time as the voltage was varied from 4 to 12 V, and (ii) a photography of the temperature distribution obtained by IR camera when 12 V was applied for 600 s. b) Pictures describing quality test of the SHE heater (520 mm × 310 mm) on the custom-designed test bed; (i) general setting of the test with a normal glass and transparent heater glass placed in front of each orchid before running a test, (ii) fog was generated on each of the window using moisturized hot air flow, (iii) defogging was carried out on the SHE heater glass for 50 s at 12 V, and (iv) temperature profile of the two glasses when defog was processed. c) Picture of the windshield of a commercial automobile (Sonata in Hyundai) incorporated with SHE heater fabricated by the electroplating equipment for large area.

an added feature for efficient blocking of the UV and IR lights when it comes to applications in automobile windshield.

4. Experimental Section

Manufacturing Processes of Oxide/Metal/Oxide (OMO) Transparent Electrodes: Zn-Sn-oxide(ZTO)/Ag/ZTO transparent electrodes were fabricated using DC magnetron sputtering guns. Consecutive coatings were performed at room temperature using in-line sputtering systems on a commercial automobile windshield (Sonata Hyundai, its diagonal length of 1530 mm) as well as on small pieces of glass (100 mm × 100 mm). Base pressure was kept at 10^{-6} Torr and the working pressure was about 5 mTorr. All the sample glasses were washed before coating processes by ethanol, acetone, and DI water.

Preparation of Super Hybrid Electrode (SHE): Positive PR was coated on OMO glasses by using a slit-die coater for samples under 30 in., or by using a screen printer for large area samples. The PR thickness was controlled to range from 1.6 to 5.5 µm by optimizing various parameters including feed rate, viscosity of PR, and baking temperature and time. ZTO layer exposed by PR patterning was etched using a diluted HF solution (1% in DI water) for about 30 s. Copper grids were selectively grown on the Ag seed layer in 1.0% Cu_2SO_4 solution in DI water by the unique electroplating machine, which could generate high voltages (1.0 to 100.0 kV) on the back sides of the OMO patterned glasses.

Transparent SHE Heaters: Transparent SHE heaters for the large-scale samples (100 mm × 100 mm, 520 mm × 310 mm) and the commercial windshield (Sonata, Hyundai, diagonal length of 1530 mm) were fabricated. Side contacts of the heaters were connected to an outer power supply (TEX20-120, Toyotech). Silver paste was used for reducing contact resistance of the SHE heaters. In order to test defog performance of the SHE heaters, a custom-designed test bed system was manufactured, which was equipped with functions to transport cool and hot airs beneath a polyacrylic chamber with two openings fitting no heater glass and SHE heater glass.

Characterizations: SEM images were obtained with field emission scanning electron microscope (Hitachi, S-4800). TEM samples were prepared by focused ion beam (Hitachi FB-2100), and analyzed by field emission transmission electron microscope (JEOL, JEM-2100F HR). XRD (Rigaku, SmartLab) was used for analyzing the crystallographic properties of the copper grids, where CuKα (λ = 0.154054 nm) was used. Large area inspection on the sample was carried out using optical microscope (Olympus, STM-6). Optical transmittance was measured by UV–vis–IR spectrophotometer (Hitachi U-3501), where the wavelength ranged from 300 to 2000 nm. Sheet resistances of the SHE samples were measured by a four-point probe (4D, 280DI). The temperatures of SHE heaters were measured by an IR-temperature camera (Fluke, Ti480).

Supporting Information

Supporting Information is available from the Wiley Online Library or from the author.

Acknowledgements

This work was supported by R&D project of Ministry of Science, ICT and Future Planning [KOITA-2016-2, Development of core-technology on transparent heating glass with auto fog-clear function for smart car].

Conflict of Interest

The authors declare no conflict of interest.

Keywords

automobile windshield, hybrid electrodes, metal grids, OMO, transparent heaters

Received: October 22, 2018
Revised: January 8, 2019
Published online: February 12, 2019

[1] K. Ellmer, *Nat. Photonics* **2012**, *6*, 809.
[2] R. Gupta, K. K. M. Rao, S. Kiruthika, G. U. Kulkarni, *ACS Appl. Mater. Interfaces* **2016**, *84*, 12559.
[3] T. Markevicius, N. Olsson, R. Furferi, H. Meyer, *J. Appl. Sci.* **2012**, *12*, 211.
[4] T. Minami, *Semicond. Sci. Technol.* **2005**, *20*, S35.
[5] K. Im, K. Cho, J. Kim, S. Kim, *Thin Solid Films* **2010**, *518*, 3960.
[6] J. H. Kim, B. D. Ahn, C. H. Kim, K. A. Jeon, H. S. Kang, S. Y. Lee, *Thin Solid Films* **2008**, *516*, 1330.
[7] D. Jung, M. Han, G. S. Lee, *J. Vac. Sci. Technol., B* **2014**, *32*, 04E105.
[8] H.-S. Jang, S. K. Jeon, S. H. Nahm, *Carbon* **2011**, *49*, 111.
[9] T. J. Kang, T. Kim, S. M. Seo, Y. J. Park, Y. H. Kim, *Carbon* **2011**, *49*, 1087.
[10] Y.-H. Yoon, J.-W. Song, D. Kim, J. Kim, J.-K. Park, S.-K. Oh, C.-S. Han, *Adv. Mater.* **2007**, *19*, 4284.
[11] Z. P. Wu, J. N. Wang, *Phys. E* **2009**, *42*, 77.
[12] J. J. Bae, S. C. Lim, G. H. Han, Y. W. Jo, D. L. Doung, E. S. Kim, S. J. Chae, T. Q. Huy, N. V. Luan, Y. H. Lee, *Adv. Funct. Mater.* **2012**, *22*, 4819.
[13] J. Kang, H. Kim, K. S. Kim, S.-K. Lee, S. Bae, J.-H. Ahn, Y.-J. Kim, J.-B. Choi, B. H. Hong, *Nano Lett.* **2011**, *11*, 5154.
[14] D. Sui, Y. Huang, L. Huang, J. Liang, Y. Ma, Y. Chen, *Small* **2011**, *7*, 3186.
[15] J. Lee, P. Lee, H. B. Lee, S. Hong, I. Lee, J. Yeo, S. S. Lee, T.-S. Kim, D. Lee, S. H. Ko, *Adv. Funct. Mater.* **2013**, *23*, 4171.
[16] T. Y. Kim, Y. W. Kim, H. S. Lee, H. Kim, W. S. Yang, K. S. Suh, *Adv. Funct. Mater.* **2013**, *23*, 1250.
[17] H. Lu, D. Zhang, J. Cheng, J. Liu, J. Mao, W. C. H. Choy, *Adv. Funct. Mater.* **2015**, *25*, 4211.
[18] S. Ye, A. R. Rathmell, Z. Chen, I. E. Stewart, B. J. Wiley, *Adv. Mater.* **2014**, *26*, 6670.
[19] X.-Y. Zeng, Q.-K. Zhang, R.-M. Yu, C.-Z. Lu, *Adv. Mater.* **2010**, *22*, 4484.
[20] S. Hong, H. Lee, J. Lee, J. Kwon, S. Han, Y. D. Suh, H. Cho, J. Shin, J. Yeo, S. H. Ko, *Adv. Mater.* **2015**, *27*, 4744.
[21] A. R. Madaria, A. Kumar, C. Zhou, *Nanotechnology* **2011**, *22*, 245201.
[22] Y. Jang, J. Kim, D. Byun, *J. Phys. D: Appl. Phys.* **2013**, *46*, 155103.
[23] H.-J. Kim, S.-H. Lee, J. Lee, E.-S. Lee, J.-H. Choi, J.-H. Jung, J.-Y. Jung, D.-G. Choi, *Small* **2014**, *10*, 3767.
[24] B. Sciacca, J. Groep, A. Polman, E. C. Garnett, *Adv. Mater.* **2016**, *28*, 905.
[25] A. Khan, S. Lee, T. Jang, Z. Xiong, C. Zhang, J. Tang, L. J. Guo, W.-D. Li, *Small* **2016**, *12*, 3021.
[26] H. Wu, D. Kong, Z. Ruan, P.-C. Hsu, S. Wang, Z. Yu, T. J. Carney, L. Hu, S. Fan, Y. Cui, *Nature Nanotechnol.* **2013**, *8*, 421.
[27] H.-G. Im, B. W. An, J. Jin, J. Jang, Y.-G. Park, J.-U. Park, B.-S. Bae, *Nanoscale* **2016**, *8*, 3916.
[28] H. Wu, L. Hu, M. W. Rowell, D. Kong, J. J. Cha, J. R. Mcdonough, J. Zhu, Y. Yang, M. D. McGehee, Y. Cui, *Nano Lett.* **2010**, *10*, 4242.
[29] B. Han, K. Pei, Y. Huang, X. Zhang, Q. Rong, Q. Lin, Y. Guo, T. Sun, C. Guo, D. Carnahan, M. Giersig, Y. Wang, J. Gao, Z. Ren, K. Kempa, *Adv. Mater.* **2014**, *26*, 873.

[30] K. D. M. Rao, G. U. Kulkarni, *Nanoscale* **2014**, *6*, 5645.
[31] S. Kiruthika, R. Gupta, A. Anand, A. Kumar, G. U. Kulkarni, *ACS Appl. Mater. Interfaces* **2015**, *7*, 27215.
[32] T. Tokuno, M. Nogi, J. Jiu, T. Sugahara, K. Suganuma, *Langmuir* **2012**, *28*, 9298.
[33] K.-W. Seo, Y.-J. Noh, S.-I. Na, H.-K. Kim, *Sol. Energy Mater. Sol. Cells* **2016**, *155*, 51.
[34] J.-A. Jeong, J. Kim, H.-K. Kim, *Sol. Energy Mater. Sol. Cells* **2011**, *95*, 1974.
[35] J. Kang, Y. Jang, Y. Kim, S.-H. Cho, J. Suhr, B. H. Hong, J.-B. Choi, D. Byun, *Nanoscale* **2015**, *7*, 6567.
[36] D. Lee, H. Lee, Y. Ahn, Y. Lee, *Carbon* **2015**, *81*, 439.
[37] X. He, R. He, Q. Lan, W. Wu, F. Duan, J. Xiao, M. Zhang, Q. Zeng, J. Wu, J. Liu, *Materials* **2017**, *10*, 220.
[38] T. Qiu, B. Lao, M. Liang, J. Ning, B. Wang, X. Li, L. Zhi, *Carbon* **2015**, *81*, 232.
[39] S.-B. Yang, H. Choi, D. S. Lee, C.-G. Choi, S.-Y. Choi, I.-D. Kim, *Small* **2015**, *11*, 1193.
[40] B. W. An, B. G. Hyun, S.-Y. Kim, M. Kim, M.-S. Lee, K. Lee, J. B. Koo, H. Y. Chu, B.-S. Bae, J.-U. Park, *Nano Lett.* **2014**, *14*, 6322.
[41] S. An, H. S. Jo, D.-Y. Kim, H. J. Lee, B.-K. Ju, S. S. A-Deyab, J.-H. Ahn, Y. Qin, M. T. Swihart, A. L. Yarin, S. S. Yoon, *Adv. Mater.* **2016**, *28*, 7149.
[42] J. Jang, H.-G. Im, J. Jin, J. Lee, J.-Y. Lee, B.-S. Bae, *ACS Appl. Mater. Interfaces* **2018**, *8*, 27035.
[43] G. Fleury, S. Belliot, N. Nadaud, *US Patent*, **2011**, US 7972713.
[44] E.-H. Ko, H.-J. Kim, S.-J. Lee, J.-H. Lee, H.-K. Kim, *RSC Adv.* **2016**, *6*, 46634.
[45] M. Girtan, *Sol. Energy Mater. Sol. Cells* **2012**, *100*, 153.
[46] B. D. Cullity, *Elements of X-Ray Diffraction*, 2nd ed., Addison-Wesley, Reading, MA **1978**, p. 102.